

Ref. 4, these modes correspond to  $K=0$  vibrations, i.e., they are optical modes. A more detailed calculation is now in progress to derive a more realistic model for  $I_2$ , taking into account these optical modes as Einstein oscillators.

The departure from linearity ( $\sim 15\%$ ) in the  $I_2$  curve at low temperatures is not yet understood. It could be due either to a slight saturation (for this case the dip is not proportional to  $f'$ ) or to a phase transition.

Experiments will be performed at lower temperatures to clarify this point.

#### ACKNOWLEDGMENTS

We wish to thank S. Alexander, Y. Disatnik, P. Hillman, H. J. Lipkin, and I. Pelah for illuminating discussions. We are grateful to Y. Regev for his collaboration in the electronics system.

### Magnetic Structures of Metallic Erbium\*

J. W. CABLE, E. O. WOLLAN, W. C. KOEHLER, AND M. K. WILKINSON

*Solid State Division, Oak Ridge National Laboratory, Oak Ridge, Tennessee*

(Received 1 June 1965)

Single-crystal neutron-diffraction data were obtained for metallic erbium at sample temperatures from 4.2 to 298°K. Three distinct regions of long-range magnetic order were observed. In the high-temperature region (52–80°K) the ordered moments are confined to the  $c$ -axis direction and are sinusoidally modulated with a modulation wavelength of  $3.5c_0$ . The amplitude of this modulation saturates at 52°K with  $\mu_z(\text{max}) = 7.6 \mu_B/\text{Er}^{3+}$ . Below 52°K the basal-plane component of the moment begins to order, and a third-order modulation along the  $c$  axis is observed. These effects are interpreted on the basis of a squared elliptical spiral with its major axis tilted relative to the crystal  $c$  axis. However, the structural details in this region are obscured by a temperature variation of the modulation wavelength and by the incommensurability of the modulation and the lattice. In the low-temperature region (4.2–20°K) a ferromagnetic spiral structure is indicated. At saturation the ferromagnetic  $c$ -axis component is  $7.9 \mu_B/\text{Er}^{3+}$  and the spiral basal-plane component is  $4.3 \mu_B/\text{Er}^{3+}$ . The total ordered moment is then the free-ion value of  $9.0 \mu_B/\text{Er}^{3+}$ .

#### INTRODUCTION

THE neutron-diffraction study which revealed many of the magnetic structural details of metallic erbium has up to now been reported only partially in a brief communication,<sup>1</sup> and we give here a complete report of these results. As with the other rare-earth elements it was necessary to make the measurements on single crystals in order to determine the rather complicated magnetic structure properties. This became apparent in some earlier powder-diffraction measurements<sup>2</sup> in which the existence of both an antiferromagnetic phase below 80°K and the development of ferromagnetism at lower temperatures was observed. These results were then consistent with previous magnetization measurements<sup>3</sup> which had indicated the onset of antiferromagnetic ordering at 80°K and a transition to ferromagnetism at 20°K. Specific-heat measurements<sup>4</sup> had indicated anomalies at these temperatures and also at 53°K. The nature of these transitions were determined in the single-crystal neutron-

diffraction studies which we report here. The most significant aspect of this study was undoubtedly the first definite observation of a modulated-moment type of structure as contrasted with the more common spiral type.

#### EXPERIMENTAL

The magnetic and thermal data indicated that neutron measurements were required in the 4.2- to 80°K region. Since the previously described<sup>5</sup> low-temperature goniometer was designed for operation in the 1.3- to 4.2°K region it was necessary to modify the goniometer for this experiment. This was done by enclosing the crystal mount and control-rod mechanism in an exchange gas chamber and by the incorporation of a heater coil and a calibrated copper-constantan thermocouple on the Al shaft above the crystal mount. With the exchange gas chamber evacuated and with no heat input the equilibrium temperature was 20°K, while with heat input the sample temperature could be raised to liquid-nitrogen temperature without the production of a prohibitive helium loss rate. It was possible to obtain temperatures below 20°K by the introduction of helium exchange gas into the chamber.

The metallic erbium single crystal was a pillar of

\* Research sponsored by the U. S. Atomic Energy Commission under contract with the Union Carbide Corporation.

<sup>1</sup> J. W. Cable, E. O. Wollan, W. C. Koehler, and M. K. Wilkinson, *J. Appl. Phys.* **32**, 49S (1961).

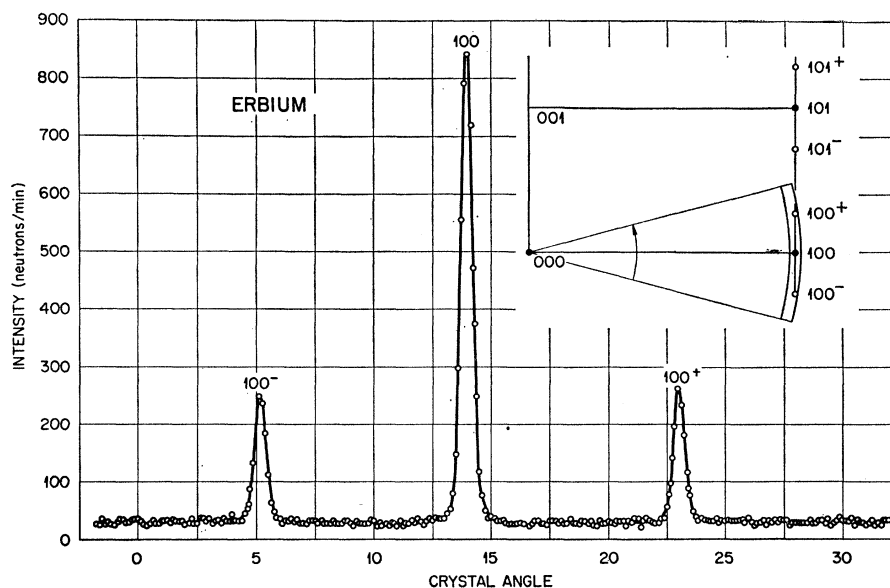
<sup>2</sup> W. C. Koehler and E. O. Wollan, *Phys. Rev.* **97**, 1177 (1955).

<sup>3</sup> J. F. Elliott, S. Legvold, and F. H. Spedding, *Phys. Rev.* **100**, 1595 (1955).

<sup>4</sup> R. E. Skochdopole, M. Griffel, and F. H. Spedding, *J. Chem. Phys.* **23**, 2258 (1955).

<sup>5</sup> E. O. Wollan, W. C. Koehler, and M. K. Wilkinson, *Phys. Rev.* **110**, 638 (1958).

FIG. 1. Crystal rocking curve about the (100) position of erbium at 75°K. The inset shows the corresponding operation in the reciprocal lattice and the indexing scheme for the satellite reflections.



rectangular cross section with dimensions of approximately 2 mm×3 mm×8 mm. The crystal  $a$  axis was oriented parallel to the long axis of the pillar, while the  $c$  axis was parallel to the 3-mm edge. The crystal was mounted in the low-temperature goniometer with the  $c$  axis parallel to the horizontal rotation axis so that it was possible to bring into Bragg reflection position all of the reflections required for structural considerations with rotation of the pillar no more than 30° from the vertical position. This procedure not only minimized the effective path length of the neutron beam through the crystal, thereby producing the maximum intensities, but also simplified the correction for absorption in the analysis of the magnetic reflection intensities.

The integrated intensity of a Bragg reflection from a mosaic crystal is given by

$$E_{hkl} = KI_0 A_{hkl} |F_{hkl}|^2 e^{-2W} / \sin 2\theta,$$

in which  $KI_0$  is an instrumental constant,  $A_{hkl}$  is the absorption correction,  $F_{hkl}$  is the structure amplitude, and  $e^{-2W}$  is the Debye-Waller correction for thermal motion. For intercomparison of the room temperature data, the  $A_{hkl}$  values were calculated with the Busing and Levy program<sup>6</sup> and the Debye-Waller corrections were made with a Debye characteristic temperature of 170°K. The internal consistency of 3% obtained for the nuclear intensities showed that extinction was not a serious problem with this crystal.

When the crystal was cooled below the Néel temperature, magnetic reflections were observed as satellites of the nuclear reflections. This is illustrated in Fig. 1 which shows a rocking curve about the (100) position at a sample temperature of 75°K. The inset shows the

corresponding operation in the reciprocal lattice and illustrates the indexing scheme of the  $hkl^\pm$  satellites of an  $hkl$  reflection. The intensities and positions of these satellites varied with temperature and these variations are illustrated in Fig. 2. This figure shows rocking curves in the (100<sup>+</sup>) region which were obtained with increasing sample temperature. The main satellite (100<sup>+</sup>) moves to higher angles with increasing temperature, while the less intense satellite moves to smaller angles. This behavior indicates that these are satellites of different reflections, and leads to the identification of the smaller reflection as the third-order satellite of the (101). In the following discussions, third-order satellites will be designated by  $(hkl^{\pm 3})$ .

The occurrence of satellite reflections shows a periodicity of the ordered magnetic moments different from that of the atomic distribution. The vector in reciprocal space which defines the displacement of the satellite reflection from the corresponding normal lattice reflection may be considered the wave vector of the magnetic-moment distribution. Throughout the magnetically ordered regions, this wave vector was observed parallel to the  $b_2$  direction which corresponds to a  $c$ -axis modulation of the moment density in real space. The modulation wavelength varied with temperature as shown in Fig. 3(d). The wavelength is constant at  $3.5C_0$  from 80 to 50°K, increases slowly down to 20°K and then abruptly increases to about  $4.1C_0$  (where  $C_0$  is the lattice spacing in the  $C$  direction). This behavior was not reversible, but rather there was an appreciable thermal hysteresis in the 20- to 50-°K region. This is shown by the arrows on the curves which indicate the direction of temperature change through this region.

Also shown in Fig. 3 are the temperature variations of the intensities of some important reflections. The

<sup>6</sup> W. R. Busing and H. A. Levy, Acta Cryst. **10**, 180 (1957).

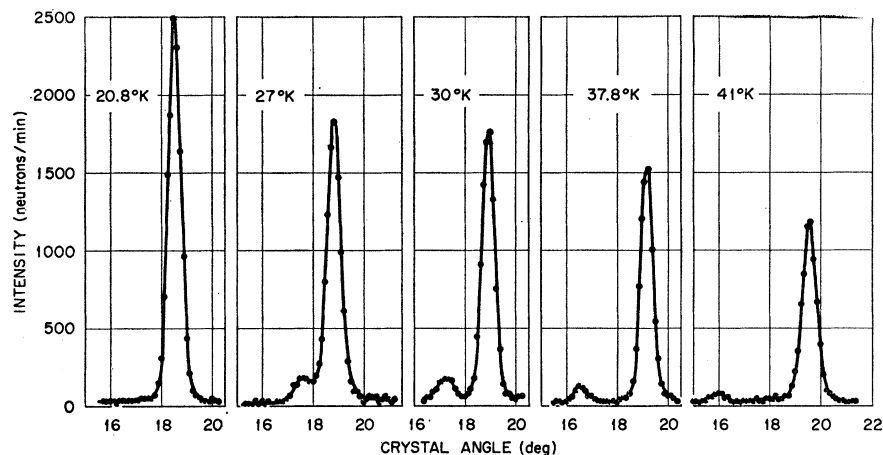


FIG. 2. Thermal behavior of the  $(100^+)$  and  $(101^{-3})$  satellite reflections of erbium.

$(100^+)$  was first observed at  $80^\circ\text{K}$ ; the intensity increased as the sample was cooled to  $20^\circ\text{K}$  and then decreased abruptly as the sample was cooled below  $20^\circ\text{K}$ . There was an appreciable thermal hysteresis loop in the  $20$ - to  $30^\circ\text{K}$  region. The origin of this loop is associated with the temperature variation of the modulation wavelength. On warming, the wavelength remains quite close to  $4.0 C_0$  from  $20$  to  $25^\circ\text{K}$ . At that wavelength the  $(100^+)$  and the  $(101^{-3})$  are superimposed (see Fig. 2) and the satellite gains intensity. On cooling, this superposition is not attained and the intensity remains low. It is of interest to note that this thermal hysteresis was not observed in the intensity of the  $(110^+)$ . This is to be expected since the  $(111)$  reflection is forbidden and consequently there is no  $(111^{-3})$  reflection.

The  $(002^-)$  satellite was not observed until the sample was cooled below  $52^\circ\text{K}$ . The intensity followed the usual saturation curve down to  $20^\circ\text{K}$  and then abruptly

increased. There also appeared at about  $50^\circ\text{K}$  a series of third-order satellites and their thermal behavior is indicated by the curve labelled  $(101^{-3})$ . These reflections seemed to disappear below  $20^\circ\text{K}$ . Finally, the behavior of the normal lattice reflections is indicated by the  $(110)$  curve which remains constant to  $20^\circ\text{K}$  and then increases discontinuously on cooling below  $20^\circ\text{K}$ . These intensity data clearly show a different type of magnetic order associated with each of three rather distinct temperature regions. The first of these is the  $52$ - to  $80^\circ\text{K}$  region in which there are first-order satellites of all reflections except the  $00l$  reflections. In the second region,  $20$ - to  $52^\circ\text{K}$ , there are first- and third-order satellites of the  $hkl$  reflections and first-order satellites of the  $00l$  reflections. The third region,  $4.2$  to  $20^\circ\text{K}$ , is characterized by first-order satellites of all reflections along with a strong ferromagnetic contribution to the normal lattice reflections. The structural considerations will be presented separately for each region.

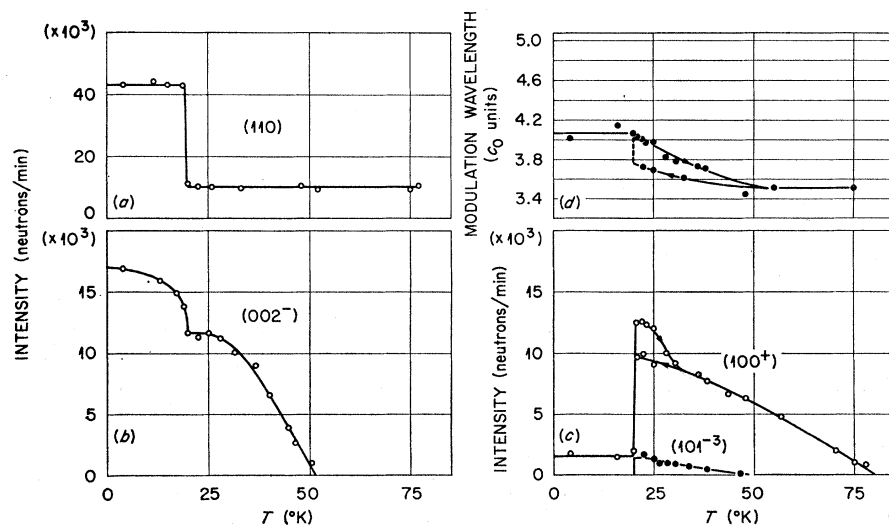


FIG. 3. Temperature variation of the modulation wavelength and the intensities of some important reflections for erbium. The arrows indicate cooling or warming through those regions with thermal hysteresis.

### The Low-Temperature Region (4.2 to 20°K)

In this region the normal lattice reflections exhibit a strong ferromagnetic component and in addition there are first-order satellites of all reflections. The 00*l* zone was scanned in a search for higher order satellites and to 0.3% of the 000<sup>+</sup> intensity none was observed. To that extent then, the moment modulation may be considered to have only one component. Two structures are then possible: the ferromagnetic spiral and a type of fan structure. The ferromagnetic spiral may be described as:

$$\begin{aligned}\mu_{ix} &= \mu \sin \gamma \cos 2\pi \tau \cdot \mathbf{R}_i, \\ \mu_{iy} &= \mu \sin \gamma \sin 2\pi \tau \cdot \mathbf{R}_i, \\ \mu_{iz} &= \mu \cos \gamma;\end{aligned}$$

and the fan-type structure as

$$\begin{aligned}\mu_{ix} &= \mu \sin \gamma \cos 2\pi \tau \cdot \mathbf{R}_i, \\ \mu_{iy} &= 0, \quad \mu_{iz} = \mu \cos \gamma;\end{aligned}$$

in which  $\tau$  is the modulation wave vector,  $\mathbf{R}_i$  is the position vector of the *i*th localized spin, and  $\gamma$  is the semiapex angle of the spiral or fan. For either of these moment configurations the ferromagnetic intensities depend only on the unmodulated *z*-axis component of the moment. The square of the structure amplitude is

$$F_{hkl}^2(\text{mag}) = 0.0725 \mu^2 \cos^2 \gamma q^2 f^2 G_{hkl}^2$$

in which  $q$  is the magnetic interaction vector,  $f$  is the magnetic form factor, and  $G_{hkl}$  is the geometrical structure factor. Intensities were obtained for a series of  $hk0$  reflections at 4.2°K and just above the Curie temperature at 21°K. The 21°K data were corrected for thermal motion by use of a Debye characteristic temperature of 160°K and subtracted from the 4.2°K data to yield the ferromagnetic intensities. The results are given in Table I along with values of  $\mu f \cos \gamma$  which were obtained by normalization to an erbium scattering amplitude of  $0.79 \times 10^{-12}$  cm. These form-factor data are shown in Fig. 4. The solid curve is the best fit of the

TABLE I. Analysis of the ferromagnetic  $hk0$  intensities at 4.2°K.

$hkl$	$F_{hkl}^2(\text{mag})^a$				
	$F_{hkl}^2(\text{nuc})$	$\mu^2 f^2 \cos^2 \gamma^b$	$\mu f \cos \gamma$	$f^c$	$\sin \theta / \lambda$
100	$5.50 \pm 0.12$	47.3	6.88	$0.869 \pm 0.013$	0.162
200	$3.23 \pm 0.07$	27.8	5.27	$0.666 \pm 0.010$	0.325
300	$1.37 \pm 0.03$	11.8	3.44	$0.434 \pm 0.006$	0.487
400	$0.72 \pm 0.09$	6.2	2.49	$0.314 \pm 0.019$	0.649
500	$0.25 \pm 0.05$	2.2	1.48	$0.187 \pm 0.019$	0.811
110	$3.32 \pm 0.06$	28.6	5.35	$0.676 \pm 0.010$	0.281
220	$1.16 \pm 0.03$	10.0	3.16	$0.399 \pm 0.008$	0.562
410	$0.41 \pm 0.02$	3.5	1.87	$0.236 \pm 0.008$	0.743

<sup>a</sup>  $F_{hkl}^2(\text{mag}) = \frac{(E_{hkl}^{2\omega})_{4.2^\circ\text{K}} - (E_{hkl}^{2\omega})_{21^\circ\text{K}}}{(E_{hkl}^{2\omega})_{21^\circ\text{K}}}$ ,  $\theta_D = 160^\circ\text{K}$ .

<sup>b</sup>  $F_{hkl}^2(\text{mag}) = 0.0725 \mu^2 q^2 f^2 \cos^2 \gamma G_{hkl}^2$ ,  $q^2 = 1$ ,  $F_{hkl}^2(\text{nuc}) = b_{\text{Er}^{3+}} G_{hkl}^2$ ,  $b_{\text{Er}^{3+}} = 0.79 \times 10^{-12}$  cm.

<sup>c</sup> Assumes  $\mu \cos \gamma = 7.92 \mu_B$  per  $\text{Er}^{3+}$  ion.

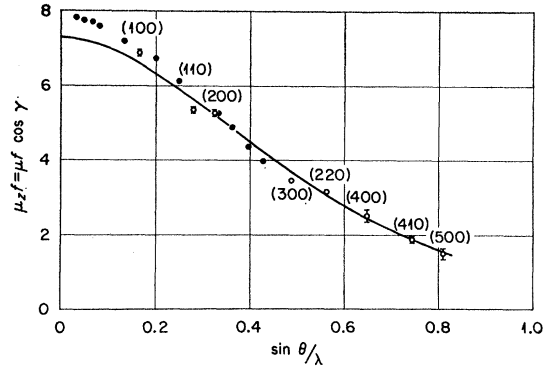


FIG. 4. Erbium form factor data. The open points are from the  $hk0$  ferromagnetic reflections at 4.2°K. The solid points represent the  $\text{Er}_2\text{O}_3$  paramagnetic scattering form factor data (Ref. 9) scaled to  $7.92 \mu_B/\text{Er}^{3+}$  as obtained by bulk magnetization measurements (Ref. 8). The solid curve is the best fit of the erbium ( $hk0$ ) data to the calculated  $\text{Er}^{3+}$  form factor (Ref. 7).

calculated<sup>7</sup> free-ion form factor to the data. In the forward direction, this corresponds to a localized moment of  $7.3 \mu_B/\text{Er}^{3+}$  for the *z*-axis component. This is appreciably smaller than the magnetization value of  $7.92 \mu_B$ <sup>8</sup> so that the use of this form factor would indicate a conduction-electron polarization of about  $0.6 \mu_B/\text{Er}^{3+}$  in the magnetization experiment. There are, however, other experimental data that indicate a more rapidly decreasing form factor for the localized  $\text{Er}^{3+}$  moment. These are the  $\text{Er}_2\text{O}_3$  paramagnetic scattering data of Koehler and Wollan.<sup>9</sup> Their form-factor data, renormalized to  $7.92 \mu_B$ , are shown as the solid points in Fig. 4. The convergence of these points onto the curve which describes the higher-angle data for the metal suggests that the  $7.9 \mu_B$  observed in the magnetization study is also appropriate to the zero-field neutron-diffraction results. The form-factor values obtained from the ( $hk0$ ) reflections on the basis of this assumption are listed in Table I.

If the *z*-axis component of the ordered moment is  $7.9 \mu_B$  and the maximum ordered moment is  $9 \mu_B$  then the maximum *x* or *y* component is  $4.3 \mu_B$ . The fan structure can be ruled out on this basis since the observed intensity of the (002<sup>-</sup>) reflection requires an *x* component of  $5.8 \mu_B$  with the fan model. We are left then with the ferromagnetic spiral structure. For this structure

$$F_{hkl}^2 = 0.0725 \frac{1}{2} [(1 + \cos^2 \phi) / 2] \mu^2 \sin^2 \gamma f^2 G_{hkl}^2$$

in which  $\phi$  is the angle between the scattering vector and the axis of constant projection of the moments. Values of  $F_{hkl}^2$  were obtained from the observed intensities by taking magnetic to nuclear intensity ratios. The absorption and thermal-motion corrections were

<sup>7</sup> M. Blume, A. J. Freeman, and R. E. Watson, J. Chem. Phys. **37**, 1245 (1962).

<sup>8</sup> R. W. Green, S. Legvold, and F. H. Spedding, Phys. Rev. **122**, 827 (1961).

<sup>9</sup> W. C. Koehler and E. O. Wollan, Phys. Rev. **92**, 1380 (1953).

TABLE II. Analysis of the 4.2°K satellite-intensity data.

$hkl^\pm$	$F_{hkl}^{2\pm}/F_{hkl}^{2\pm a}$	$\frac{1}{2}(1+\cos^2\phi)^b$	$f^{2c}$	$\mu^2 \sin^2\gamma^d$
100 $\pm$	0.40	0.509	0.746	18.0 $\pm$ 0.5
200 $\pm$	0.22	0.503	0.440	17.5 $\pm$ 0.7
300 $\pm$	0.13	0.502	0.196	23.5 $\pm$ 1.5
110 $\pm$	0.28	0.501	0.516	18.5 $\pm$ 0.5
220 $\pm$	0.10	0.501	0.148	23.5 $\pm$ 2.4
002 $^-$	0.74	1.000	0.766	16.6 $\pm$ 0.2
002 $^+$	0.69	1.000	0.669	17.7 $\pm$ 0.3
004 $^-$	0.40	1.000	0.420	16.6 $\pm$ 0.4
004 $^+$	0.28	1.000	0.350	13.9 $\pm$ 0.5
006 $^-$	0.24	1.000	0.188	22.0 $\pm$ 1.0
006 $^+$	0.17	1.000	0.151	19.2 $\pm$ 1.1
	$\pm 0.01$			

<sup>a</sup>  $F_{hkl}^{2\pm}/F_{hkl}^{2\pm} = E_{hkl} \sin 2\theta_{hkl} / E_{hkl} \sin 2\theta_{hkl}$ .

<sup>b</sup> Assumes a regular spiral with moments in the basal plane.

<sup>c</sup> Experimental Er form factor (Table I).

<sup>d</sup>  $F_{hkl}^{2\pm} = 0.0725[(1+\cos^2\phi)/2]^{1/2} \mu^2 \sin^2\gamma^2 G_{hkl}^2$  (spiral),  
 $F_{hkl}^{2\pm} = b_{Er}^2 G_{hkl}^2$ ,  $b_{Er} = 0.79 \times 10^{-12}$  cm.

the same within 1% for the satellite reflections and the associated normal lattice reflection so that the factor,  $KI_0 A_{hkl} e^{-2w}$ , cancelled out of the intensity ratio and,

$$F_{hkl}^{2\pm} = (E_{hkl} \sin 2\theta_{hkl} / E_{hkl} \sin 2\theta_{hkl}) F_{hkl}^2.$$

The analysis of the 4.2°K satellite intensity data based on the spiral model is given in Table II. A basal-plane component of  $4.3 \mu_B/\text{Er}^{+3}$  gives reasonable agreement with these data.

### The High-Temperature Region (52 to 80°K)

This region is characterized by first-order satellites of all reflections except the 00 $l$ 's. The absence of higher order satellites indicates a sinusoidal modulation of the moments, while the absence of 00 $l$  $^\pm$  satellites indicates that the ordered moments are aligned parallel to the  $c$ -axis direction. The moment distribution may then be described by

$$\begin{aligned} \mu_{iz} &= \mu_{iy} = 0, \\ \mu_{ix} &= \mu_{\max} \sin(2\pi\tau \cdot \mathbf{R}_i + \delta), \end{aligned}$$

in which  $\delta$  is an indeterminate phase angle and  $\mu_{\max}$  is the amplitude of the modulation wave in  $\mu_B/\text{Er}^{+3}$ . The square of the structure amplitude for such an oscillating component model is given by

$$F_{hkl}^2 = 0.0725(q^2/4) \mu_{\max}^2 f^2 G_{hkl}^2.$$

The analysis for the satellite reflections observed at 52°K is given in Table III. The agreement among the  $\mu_{\max}^2$  values is sufficient to support the assumed oscillating-component model.

### The Intermediate Region (20 to 52°K)

In the intermediate region a more complicated behavior was observed than for the other two regions. There are first-order satellites of all reflections and third-order satellites of the  $hkl$  reflections. In addition, the modulation wavelength varies with temperature and shows a thermal hysteresis effect. Qualitatively,

we might envisage two related models that would produce these diffraction effects. Both are modified spirals in which the moments, when projected to a common origin, lie in a plane. The observed intensities show that the  $z$  component is larger than the  $x$  or  $y$  component so that the hodograph of the moments is not circular, as in the regular spiral, but elliptical. Presumably, this is due to crystal-field anisotropy effects which favor  $c$ -axis moment alignment in Er. The two models differ only in the orientation of the major axis of the ellipse relative to the  $c$  axis. In one model the major axis is parallel to the  $c$  axis, so that the  $x$  and  $z$  components of the moment oscillate while the  $y$  component vanishes. The  $x$  axis in the crystal would be determined by the basal-plane anisotropy, and the six-fold symmetry of that anisotropy would probably lead to domains in which the  $xz$  planes of moments assume the three preferred orientations. In the other model, the major axis of the ellipse is tilted relative to the  $c$  axis so that the  $x$  and  $y$  components of the moment execute a regular spiral. The appearance of the third-order satellites shows that neither of these descriptions is adequate and that there must be some distortion of the ellipse. Since the effect was more pronounced for the  $z$ -axis component (00 $l$  $^\pm$  were not observed), the distortions must be concentrated near the major axis of the ellipse. Unfortunately, the two models produce the same diffraction effects, and in this region where saturation has not been achieved, intensity arguments, such as those used in the 4.2- to 20-°K region, are ineffective in supporting a unique model. However, there is an anisotropy argument which supports the tilted-ellipse model. The low-temperature structure is a ferromagnetic spiral in which the basal-plane component describes a regular spiral with a turn angle of about 44°. Basal-plane anisotropy cannot be an important effect with such a structure, and is expected to be even less important in the higher temperature regions. There is, then, no reason for the restriction of the  $x$  component to specific basal-plane directions as required for the model with the major axis parallel to the  $c$  axis. For this reason, the data have been analyzed on the tilted-axis model, which has been simplified by the assumption

TABLE III. Analysis of the 52°K satellite-intensity data.

$hkl^\pm$	$F_{hkl}^{2\pm}/F_{hkl}^{2\pm a}$	$q^{2b}$	$f^{2c}$	$\mu_{\max}^2 d$
100 $\pm$	1.28	0.976	0.746	61 $\pm$ 2
200 $\pm$	0.68	0.994	0.440	54 $\pm$ 3
300 $\pm$	0.33	0.998	0.196	58 $\pm$ 5
110 $\pm$	0.87	0.992	0.516	59 $\pm$ 2
101 $^-$	0.90	0.865	0.723	53 $\pm$ 2
103 $^-$	0.31	0.309	0.491	70 $\pm$ 7
103 $^+$	0.15	0.235	0.426	53 $\pm$ 10
	$\pm 0.03$			

<sup>a</sup>  $F_{hkl}^{2\pm}/F_{hkl}^{2\pm} = E_{hkl} \sin 2\theta_{hkl} / E_{hkl} \sin 2\theta_{hkl}$ .

<sup>b</sup> Assumes moment alignment parallel to the  $c$  axis.

<sup>c</sup> Experimental Er form factor (Table I).

<sup>d</sup>  $F_{hkl}^{2\pm} = 0.0725(q^2/2) (\mu_{\max}^2/2) f^2 G_{hkl}^2$  (oscillating component),  
 $F_{hkl}^{2\pm} = b_{Er}^2 G_{hkl}^2$ ,  $b_{Er} = 0.79 \times 10^{-12}$  cm.

that the basal-plane component of the moment executes a regular spiral. This analysis is shown in Table IV for the 20-°K satellite data obtained on warming. In column 2 are the  $F^2$  values obtained by the intensity ratio method with the assumption of the erbium nuclear scattering amplitude. In column 3 are the contributions due to the ordered basal-plane components of the moment based on a regular spiral structure, the experimental form factor, and a basal-plane moment derived from the (002<sup>-</sup>) intensity. The difference between these two columns gives the  $F^2$  values associated with the  $z$ -axis component of the moment. This component has first- and third-order modulations and can therefore be written as:

$$\mu_i(z) = A_1 \cos(2\pi\tau \cdot \mathbf{R}_i + \delta) + A_3 \cos(2\pi 3\tau \cdot \mathbf{R}_i + \phi)$$

in which  $\delta$  and  $\phi$  are phase angles relative to the atomic positions. The amplitudes  $A_1$  and  $A_3$  can be determined from the intensities of the (110<sup>+</sup>) and (110<sup>+3</sup>) reflections, respectively. The values obtained were  $A_1 = 9.72 \mu_B$  and  $A_3 = 2.97 \mu_B$ . The structure is then defined by a knowledge of the two phase angles  $\delta$  and  $\phi$ . Since the maximum total moment is  $9 \mu_B$ , and the basal-plane component is  $3.6 \mu_B$ , the  $z$  component of the moment cannot exceed  $8.2 \mu_B$ . This suggests that the two cosine waves should be combined as nearly out of phase as possible. The most symmetrical phasing which satisfies the  $8.2 \mu_B$  criterion is that with  $\delta = 22\frac{1}{2}^\circ$  and  $\phi = 247\frac{1}{2}^\circ$ . For the eight atoms of the magnetic unit cell with this set of phase angles,

$$\mu_0 = -\mu_3 = -\mu_4 = \mu_7 = 7.84 \mu_B,$$

$$\mu_1 = -\mu_2 = -\mu_5 = \mu_6 = 6.46 \mu_B.$$

The  $F^2$  values calculated for this structure are given in the last column of Table IV and agree quite well with the observed values. It should be noted that the calculated  $F^2$  values for the 10 $l^\pm$  satellites are average values for (100<sup>+</sup>, 100<sup>-</sup>) and (103<sup>-</sup>, 103<sup>+</sup>) pairs. This averaging is necessary because there is no unique positive direction in the crystal and domains undoubtedly develop with equal probability in the two  $c$ -axis directions.

The 20-°K satellite data obtained on cooling are shown in Table V. Here again the basal-plane contribution has been removed on the assumption of a regular spiral and the  $F^2$  values attributed to the  $z$ -axis com-

TABLE V. Intensity data on cooling to 20°K.

$hkl$	$F_{hkl}^{\pm 2}$ <sup>a</sup>	$F_{hkl}^{\pm 2}(xy)$ <sup>b</sup>	$F_{hkl}^{\pm 2}(z)$	$\mu_z^2 G_{hkl}^{\pm 2}$ <sup>c</sup>
100 <sup>±</sup>	0.371±0.011	0.044	0.327	6.2
310 <sup>±</sup>	0.078±0.005	0.008	0.070	7.3
101 <sup>-</sup>	0.955±0.029	0.143	0.812	18.0
101 <sup>+</sup>	0.865±0.026	0.156	0.709	21.4
103 <sup>-</sup>	0.337±0.017	0.144	0.193	17.6
110 <sup>±</sup>	1.030±0.010	0.121	0.909	24.6
220 <sup>±</sup>	0.293±0.007	0.034	0.259	23.9
300 <sup>±</sup>	0.406±0.008	0.046	0.360	25.5
101 <sup>-3</sup>	0.051±0.005		0.051	1.0
110 <sup>+3</sup>	0.050±0.005		0.050	1.5

$$^a F_{hkl}^{\pm 2} = (E_{hkl}^{\pm} \sin 2\theta_{hkl} / E_{hkl} \sin 2\theta_{hkl}) F_{hkl}^{\pm 2}, F_{hkl}^{\pm 2} = b_{Er}^2 G_{hkl}^{\pm 2},$$

$$b_{Er} = 0.79 \times 10^{-12} \text{ cm.}$$

$$^b F_{hkl}^{\pm 2}(xy) = 0.0725 \frac{1}{2} [(1 + \cos^2\phi) / 2] \mu_{xy}^2 f^2 G_{hkl}^{\pm 2},$$

$$\mu_{xy}^2 = \mu_x^2 = \mu_y^2 = (I_{002}^{-20^\circ\text{K}} / I_{002}^{-4.2^\circ\text{K}}) (\mu^2 \sin^2\gamma)_{4.2^\circ\text{K}} = 0.68 (18.8) = 12.8.$$

$$^c F_{hkl}^{\pm 2}(z) = 0.0725 q^2 f^2 \mu_z^2 G_{hkl}^{\pm 2}.$$

ponent are given in column 4. These have been converted to  $\mu_z^2 G_{hkl}^{\pm 2}$  values in the last column. Again, the amplitudes of the first- and third-order modulation waves can be obtained from the 110<sup>+</sup> and 110<sup>+3</sup> intensities. These are:  $A_1 = [4(24.6)]^{1/2} = 9.92 \mu_B$  and  $A_3 = [4(1.5)]^{1/2} = 2.45 \mu_B$ . As in the previous case, these waves must combine to yield moments at the lattice sites no larger than  $8.2 \mu_B$ . The structure in this region must be quite similar to that described in the preceding paragraph, but is difficult to describe in detail because the modulation waves are incommensurate with the lattice.

## DISCUSSION

The neutron-diffraction data show the existence of three regions of long range magnetic order for metallic erbium. In the high-temperature region (52 to 80°K), the ordered moments are confined to the  $c$ -axis direction and are sinusoidally modulated with a modulation wavelength of  $3.5 C_0$ . This is the expected<sup>10-12</sup> structure for a system with an isotropic exchange interaction which imposes the modulation and a crystal field anisotropy which gives preference for moment alignment parallel to the  $c$  axis. This structure has also been observed for thulium.<sup>13</sup> As the sample is cooled below 80°K the amplitude of the modulation wave increases until the maximum  $c$ -axis component of the moment consistent with the crystal-field anisotropy is attained. This occurs at 52°K with  $\mu_z(\text{max}) = 7.6 \mu_B/\text{Er}^{3+}$ . (This is the amplitude of the modulation and not necessarily the magnitude of any localized moment since the relative phases of the modulation and the atomic positions are not determined in this experiment.) Below 52°K there is a departure from the simple sinusoidal modulation of the  $z$ -axis component which results in a squaring of the modulation. In addition, an ordered basal-plane component of the moment develops. The

TABLE IV. Analysis of the 20°K (warming) intensity data.

$hkl$	$F_{hkl}^{\pm 2}$ <sup>a</sup>	$F_{hkl}^{\pm 2}(xy)$ <sup>b</sup>	$F_{hkl}^{\pm 2}(z)$	$F_{hkl}^{\pm 2}(z)$ (calc) <sup>c</sup>
100 <sup>±</sup>	0.471±0.014	0.044	0.427±0.014	0.398
103 <sup>-</sup>	0.332±0.017	0.144	0.188±0.017	0.199
110 <sup>±</sup>	0.992±0.010	0.121	0.871±0.010	(0.871)
110 <sup>+3</sup>	0.075±0.008		0.075±0.008	(0.075)

$$^a F_{hkl}^{\pm 2} = (E_{hkl}^{\pm} \sin 2\theta_{hkl} / E_{hkl} \sin 2\theta_{hkl}) F_{hkl}^{\pm 2}, F_{hkl}^{\pm 2} = b_{Er}^2 G_{hkl}^{\pm 2},$$

$$b_{Er} = 0.79 \times 10^{-12} \text{ cm.}$$

$$^b F_{hkl}^{\pm 2}(xy) = 0.0725 \frac{1}{2} [(1 + \cos^2\phi) / 2] \mu_{xy}^2 f^2 G_{hkl}^{\pm 2},$$

$$\mu_{xy}^2 = \mu_x^2 = \mu_y^2 = (I_{002}^{-20^\circ\text{K}} / I_{002}^{-4.2^\circ\text{K}}) (\mu^2 \sin^2\gamma)_{4.2^\circ\text{K}} = 0.68 (18.8) = 12.8.$$

$$^c F_{hkl}^{\pm 2}(z) = 0.0725 q^2 f^2 \mu_z^2 G_{hkl}^{\pm 2}.$$

<sup>10</sup> T. A. Kaplan, Phys. Rev. **124**, 329 (1961).

<sup>11</sup> R. J. Elliott, Phys. Rev. **124**, 346 (1961).

<sup>12</sup> H. Miwa and K. Yosida, Progr. Theoret. Phys. (Kyoto) **26**, 693 (1961).

<sup>13</sup> W. C. Koehler, J. W. Cable, E. O. Wollan, and M. K. Wilkinson, Phys. Rev. **126**, 1672 (1962).

structural details in this region are obscured by the temperature variation of the modulation wavelength and the incommensurability of the modulation and the lattice. However, for the commensurate  $4.0 C_0$  structure obtained on warming through the 20- to 25°-K region, a satisfactory model has been obtained. In this model the basal-plane component assumes a spiral configuration and the  $c$ -axis component exhibits the variation:  $\mu_0 = -\mu_3 = -\mu_4 = \mu_7 = 7.84 \mu_B$  and  $\mu_1 = -\mu_2 = -\mu_5 = \mu_6 = 6.46 \mu_B$ . In the 4.2- to 20°K region a ferromagnetic spiral structure is indicated. At 4.2°K, the spiral basal-plane component is  $4.3 \mu_B$  while the ferromagnetic  $c$ -axis component is  $7.9 \mu_B$ . These yield a total ordered moment in good agreement with the  $9 \mu_B$  expected for the  $\text{Er}^{3+}$  ion. The magnetic structures of the heavy rare earth metals have been discussed by several authors<sup>10-12</sup> who conclude that the rather startling variety of observed structures can be explained by the superimposed effects of an isotropic exchange interaction which imposes the moment modulation and a temperature-

dependent crystal-field anisotropy. The exchange interaction is assumed to be of the Rudermann-Kittel type which couples localized spins by polarization of the conduction electrons. It has been shown<sup>14-16</sup> that this interaction, when applied to an hexagonal-close-packed array of localized spins in a system with three conduction electrons per atom, leads to a modulated-moment distribution with a modulation wavelength of about  $3.6 C_0$  in remarkable agreement with these observations.

#### ACKNOWLEDGMENTS

We would like to express our appreciation to Professor S. Legvold and Professor F. H. Spedding of Iowa State University for the loan of the single-crystal samples used in this investigation.

<sup>14</sup> E. J. Woll and S. J. Nettel, *Phys. Rev.* **123**, 796 (1961).

<sup>15</sup> K. Yosida and A. Watabe, *Progr. Theoret. Phys. (Kyoto)* **28**, 361 (1962).

<sup>16</sup> T. A. Kaplan and D. H. Lyons, *Phys. Rev.* **129**, 2072 (1963).

## Theory of the Anisotropic Energy Gap in Superconducting Lead\*†

ALAN J. BENNETT‡

*Department of Physics and Institute for the Study of Metals, University of Chicago, Chicago, Illinois*

(Received 15 July 1965)

The energy gap of a model anisotropic superconductor is considered. This model calculation forms the basis of a more realistic theoretical consideration of the energy gap of superconducting Pb, one in which the phonon density of states is the principal source of gap anisotropy. The effect of energy-band structure, important only near Brillouin-zone boundaries, is included as a perturbation. The phonon density of states is calculated from the experimental dispersion curves and singularities—present in the special density of states entering the superconductivity problem—are discussed. The phonon density of states and the isotropic gap solution obtained by previous workers are used to calculate the anisotropic part of the energy gap. The double gap,  $2\Delta$ , is found to have an absolute maximum of 2.86 meV in the  $[100]$  direction, and an absolute minimum of 2.55 meV in the  $[110]$  direction. Ten other maxima, minima, and saddle points are listed. The effect of the energy-gap anisotropy on electron-tunneling, electromagnetic-absorption, and acoustic-attenuation experiments is predicted.

### I. INTRODUCTION

IN the original Bardeen-Cooper-Schrieffer<sup>1</sup> (BCS) formulation of the theory of superconductivity, a constant effective electron-electron interaction and spherical Fermi surface were assumed. The energy-gap equation, when solved under these assumptions, yielded an isotropic solution, i.e., one independent of crystallographic angle. These assumptions are, of course, too drastic, as the following experiments have shown:

- (1) electromagnetic absorption in Al,<sup>2</sup> Sn,<sup>3</sup>
- (2) acoustic attenuation in Sn,<sup>4</sup> Zn,<sup>5</sup>
- (3) tunneling in Sn,<sup>6</sup> Pb.<sup>7,8</sup>

All these experiments indicate a range of energy gaps, i.e., an energy gap that varies with angle and may be different on different sheets of the Fermi surface.

<sup>2</sup> M. A. Biondi, M. P. Garfunkel, and W. A. Thompson, *Phys. Rev.* **136**, A1471 (1964).

<sup>3</sup> P. L. Richards, *Phys. Rev. Letters* **7**, 412 (1961).

<sup>4</sup> R. W. Morse, T. Olsen and J. D. Gavenda, *Phys. Rev. Letters* **3**, 15, 193 (1959); **3**, 193 (E) (1959).

<sup>5</sup> H. V. Bohm and N. H. Horowitz, *Proceedings of the Eighth International Conference on Low Temperature Physics* (Butterworths Scientific Publications, Inc., Washington, 1963).

<sup>6</sup> N. V. Zavaritskii, *Zh. Eksperim. i Teor. Fiz.* **43**, 1123 (1962) [English transl.: *Soviet Phys.—JETP* **16**, 793 (1962)].

<sup>7</sup> P. Townsend and J. Sutton, *Phys. Rev.* **128**, 591 (1962).

<sup>8</sup> G. I. Rochlin and D. H. Douglass, Jr., *Bull. Am. Phys. Soc.* **10**, 46 (1965).

\* Supported in part by the National Aeronautics and Space Administration.

† Submitted in partial fulfillment of the requirements for the degree of Doctor of Philosophy at the University of Chicago.

‡ National Science Foundation predoctoral fellow.

<sup>1</sup> J. Bardeen, L. N. Cooper, and J. R. Schrieffer, *Phys. Rev.* **108**, 1175 (1957).